SSRG International Journal of VLSI and Signal Processing
ISSN: 2394–2584 / https://doi.org/10.14445/23942584/IJVSP-V11I1P101

Volume 11 Issue 1, 1-8, Jan-April 2024

Original Article

Direct Analytical Impact of Antenna Pitch and Number of Antennas on Network Factor and Radiation Pattern in Planar Antenna Array Design

Zanga Mvodo Martin Paulin[1], Koko Same Louis Christian[2], Essiben Dikoundou Jean-François[3]

[1,2,3]*Doctoral Training Unit of Applied Science, Doctoral School of Fundamental and Applied Sciences (EDOSFA), Douala, Cameroon.*

[1]*Corresponding Author : zangamvodomartinparulin@yahoo.fr*

Received: 05 February 2024 Revised: 27 March 2024 Accepted: 11 April 2024 Published: 31 April 2024

Abstract *- In this work, we propose to study analytically the impact of inter-element distance and number of transducers on the grating factor, radiation pattern, directivity and beamwidth at HPBW power of a planar antenna array during its design. In contrast to numerical methods such as Fourrier, Capon, Shelkunnov, Tschebyschef, least square and others, the direct analytical method uses the classical beamforming mechanisms known in the basic linear Broadside array, also known as slotted arrays. These slotted arrays are the very basis of the design idea behind other existing antenna array geometries*.

Keywords *- Beamforming, End-fire, Broadside, Half-Power BeamWidth, Array factor.*

1. Introduction

Printed or integrated high-gain directional antennas receive a great deal of attention in the literature because they are so useful in practice. They find their application as essential signal transfer links, notably engraved on the surface of a metal structure such as an aircraft fuselage or a Massive MIMO sectorial [1], to name but a few. To facilitate their design, it is essential to opt for a flat, infinite surface on which the sensor is mounted. However, in certain situations, the effects of the finite size of the print circuit or the layout or ground plane must be considered in the design analysis [2]. This is the case with a linear end-fire array excited by a travelling wave current distribution. It is inevitable to realize that the finite size of the printed circuit board affects both the directivity and the orientation of the main lobe of the resulting pattern [3]. Another proven scenario is that in which a travelling-wave-fed antenna is cut on a finite-size PCB that rests on the ground plane surface, and a rough aperture is cut to support the slot. This is particularly the case with aperture slot arrays on airport tarmacs, generally used to facilitate ILS or radio beacon guidance operations in adverse weather conditions to enable aircraft taxiing, take-off, and/or landing. Various configurations of slit gratings exist [4], [5], each differentiated by the type of elementary slit. The reason for this differentiation here is that it is the slit pattern that defines the excitation mode. Direct analysis of slit gratings often induces a waveguide feed to the slits [6] - [7] or simply a slotted waveguide arrangement [8], [9]. Many recently published works closely related to planar gratings are available in the literature. Those that have caught our attention are presented in a brief analysis of this research in relation to the present study. In [10], a calculation of the resulting radiation patterns for different cases of adjacent magnetic line sources with perfectly conducting half-plane is performed. The results of this previous work have been extended and generalized to the case of arbitrary sources such as apertures and slots [6],[11]. [12] provides radiation patterns calculated for a parallel magnetic linear array of antennas mounted on a half-plane.

Here, we demonstrate that the finite distance of the array from the end of the half-plane causes the main lobe of the End-Fire array to tilt. It is this phenomenon that will later be exploited in a large planar network (Massive MIMO) via simple phase control to enable agility of said radiation pattern and thus serve a moving target. This set of advantages offered by the parallel magnetic linear array of antennas mounted on a half-plane is the reason for its choice in the rest of this work. We also assume that the coupling effect is neglected throughout the study. The main aim of this article is to make a theoretical study, in the design of a planar antenna array, of the impact of the array pitch and the number of radiating elements on the radiation pattern, the array factor, the directivity and the beam width at power loss. The geometry of the problem under consideration assumes that the printed plane or ground plane is ultra-thin to minimize coupling effects and modeled by a perfectly conducting half-plane. Each sensor in the array is rectangular in shape, arranged in

such a way as to form discrete distributions that are continuous along the linear array, in which the slots are cut on the ultra-thin, perfectly conductive ground plane.

2. Materials and Methods

2.1. Material

We used a Matlab Release 2024a (R2024a) simulation environment installed in an HP laptop with the following specifications: Intel(R) Core(TM) i5-8350U CPU @ 1.70GHz 1.90 GHz, 8.00 GB RAM, 1TB SSD hard disk, Windows 10 operating system, 64-bit.

2.2. Methods

Problem Formulation and System Modeling Consider a rectangular array of N × M parallel magnetic isotropic sensors mounted on a half-plane and spaced dx along the x-axis and dy along the y-axis, as shown in Figure 1. With θ the elevation and φ the azimuth, coupling effects are not considered, which implies that only the fields radiated by each element are considered; those stray fields created around and induced on neighbors are neglected.

We propose to observe the evolution of the radiation pattern and the grating factor in dimension 2 on the one hand and to determine the beam width at half-power HPBW, the progressive phases in the x and y directions and the directivity D (dB) on the other, when the spacing varies between 0.25 and λ along y to 0.5 λ fixed along x and vis-versa.

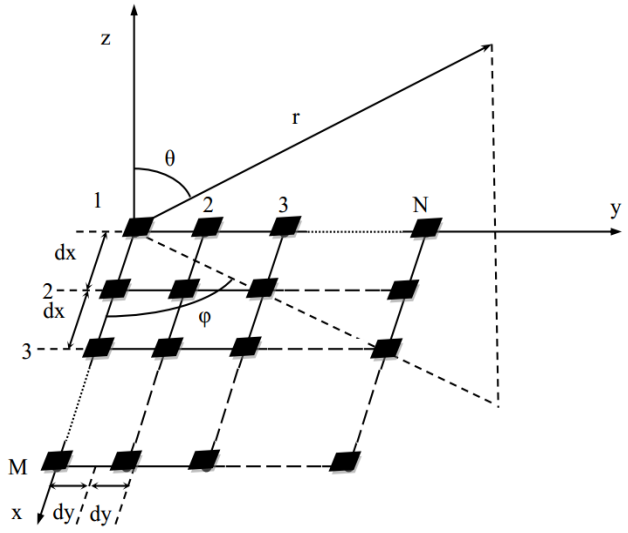

Fig.1 Rectangular array of N × M isotropic sensors mounted on a half-plane

2.3. Radiation Diagram

The n-sensor radiation diagram formula can be generalized by:

$$p(\theta,\varphi) = \frac{\left|\sum_{p=1}^{ncapt} I_p Ethet_P(\theta_p,\varphi_p).exp\left(\frac{2j\pi}{\lambda}.\vec{u}_r O\vec{O}_p\right)\right|^2 + \left|\sum_{p=1}^{ncapt} I_p Ephi_P(\theta_p,\varphi_p).exp\left(\frac{2j\pi}{\lambda}.\vec{u}_r O\vec{O}_p\right)\right|^2}{p_{norm}} \quad (1)$$

Where, for source number p, *Ethetp* and *Ephip* correspond to the a priori complex radiated fields of the source alone (or of the source in its environment if considered), which we will call the elementary diagram. Ip corresponds to the weighting or complex feed applied to source p. It represents the position of source p relative to a fixed-point O taken as the origin of the reference frame represents the orientation direction (θ,φ), common to all sources since we are in the far field. λ corresponds to the length of the wave emitted into the air. However, although we are in a planar array, it is important to remember that the analysis is performed on linear arrays following axes one after the other, and at the end, we perform a summation. For example, considering that all the sensors in the network are aligned along the y-axis, we can rewrite equation (1) as follows

$$p(\theta,\varphi) = f(\theta,\varphi)\sum_{n=1}^{ncapt} I_n exp(jk_0 \sin\theta.(y_n \cos\varphi)) \quad (2)$$

Where f (θ, φ) materializes the radiation pattern of a source, the coordinates of the source. The nth-order complex power-weighting coefficient and the resulting wave number.
Analytically, we can see from the above that, grouped in a grid, the resulting radiation pattern is the product of two terms, namely:
a-) the radiation or field produced by a single element fed by a source delivering a current at its input and
b-) a network factor that depends on the network's geometric parameters and weighted supply currents.
For a rectangular network of N × M elements, the network factor can be written as:

$$F(\theta,\varphi) = \sum_{m=1}^{M} I_{m1}\, e^{j(m-1)(kd_x \sin\theta\cos\varphi+\beta_x)} \sum_{n=1}^{N} I_{n1} e^{j(n-1)(kd_y \sin\theta\sin\varphi+\beta_y)} \quad (3)$$

As this type of structure is commonly used in scanning radars and Massive MIMO for 5G mobile applications such as IoT with drones or when a user is mobile, it may be necessary to steer the beam of the antenna structure in a specific direction or at a specific angle without mechanically moving the entire structure. To do this, simply act on the progressive phases and as follows:

$$\beta_x = -kd_x \sin\theta_0 \sin\varphi_0 \quad (4)$$

$$\beta_y = -kd_y \sin\theta_0 \sin\varphi_0 \quad (5)$$

Where represent the desired illumination angles.

2.4. Beam width

Finding the beamwidth of a planar array of uniform amplitude is no easy task. This article describes a very simple procedure that can be used to calculate the parameters for large arrays whose scan maximum is not too far from a Broadside array. The method consists of using the results of the beam broadening factor of a linear array of uniform amplitude distribution, considering that the maximum of the conical main lobe of the array is oriented towards the max of a

Broadside array (-90) To define a beam width, two planes are chosen.
a-) One in the plane of the elevation defined by the angle
b-) The other plane is perpendicular to it.
For a large array, with a maximum close to that of a Broadside array, the half-power beamwidth in the plane of elevation is given approximately by:

$$\theta_h = \sqrt{\frac{1}{cos^2\theta_0\left[\theta^{-2}{}_{x0}cos^2\varphi_0+\theta^{-2}{}_{y0}sin^2\varphi_0\right]}} \quad (6)$$

Where represents the half-power beamwidth of a Broadside linear array of M elements. Similarly, it represents the half-power beamwidth of a Broadside linear array of N elements. The values of and can be obtained using the previous results.
a-) For a uniform distribution, the values of and can be obtained using, respectively, the lengths and reading the values on the abacus in Figure 2.
b-) The same concept can be used to obtain the beamwidth of other distributions as many times as their corresponding beamwidth factors are available.

In the case of a square network (6) can be reduced to:

$$\theta_h = \theta_{x0}\, sec\,\theta_0 = \theta_{x0}\, sec\,\theta_0 \quad (6a)$$

Equation (6a) indicates that increases in beam width are proportional to An increase in beamwidth per in is consistent with the reduction in the cost of the projected domain of the grating in the pointing direction. The half-power beamwidth, in the plane perpendicular to the elevation altitude, is given by:

$$\psi_h = \sqrt{\frac{1}{\theta^{-2}{}_{x0}sin^2\varphi_0+\theta^{-2}{}_{y0}cos^2\varphi_0}} \quad (7)$$

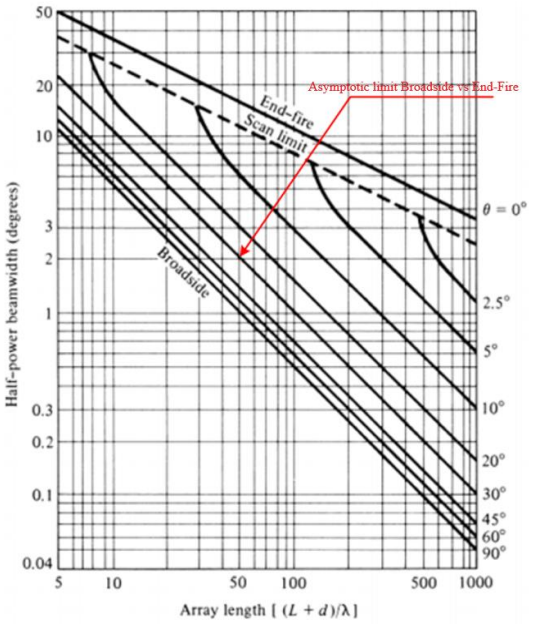

Fig. 2 HPBW curve as a function of linear network length

2.5. Directivity

The directivity of the grating factor whose main lobe is directed towards and can be defined as:

$$D_0 = \frac{4\pi[AF(\theta_0,\varphi_0)][AF(\theta_0,\varphi_0)]*lmax}{\int_0^{2\pi}\int_0^{2\pi}[AF(\theta_0,\varphi_0)][AF(\theta_0,\varphi_0)]*\sin\theta d\theta d\varphi} \quad (8)$$

Where represents the grating factor at the maximum grating length. For large planar gratings, most of which are almost Broadside, the directivity reduces to:

$$D_0 = \pi\cos\theta_0\, D_x D_y \quad (9)$$

Where and are the directivities of a Broadside linear array, and M and N are, respectively, the lengths and numbers of elements. The factor describes the decrease in directivity due to the decrease in the projected domain of the array.
In this article, we will discuss simulation results following 3 Scenarios:

- ❖ M and N even
- ❖ M and N odd
- ❖ M even and N odd
- ❖ odd M and even N

Before discussing these results, it is necessary to justify the choice of a few parameters, namely azimuth, elevation and inter-element spacing. The first two are chosen arbitrarily (φ=45°, θ=30°); on the other hand, the distance dx or dy is momentarily fixed at ½ λ because in a linear array of elements, the optimal values of the array factor and the radiation pattern, are obtained at an inter-element distance of ½ λ [13]. Based on this assumption, the expression of the radiation diagram (1) can still be written as:

$$p(\theta,\varphi) = \frac{\sin\left(\frac{N}{2}\left(\frac{2\pi dx}{\lambda}\sin\theta\cos\varphi+\Delta\emptyset x\right)\right)}{\mathrm{N}\sin\left(\frac{1}{2}\left(\frac{2\pi dx}{\lambda}\sin\theta\cos\varphi+\Delta\emptyset x\right)\right)}\cdot\frac{\sin\left(\frac{M}{2}\left(\frac{2\pi dx}{\lambda}\sin\theta\sin\varphi+\Delta\emptyset x\right)\right)}{\mathrm{M}\sin\left(\frac{1}{2}\left(\frac{2\pi dx}{\lambda}\sin\theta\sin\varphi+\Delta\emptyset x\right)\right)} \quad (10)$$

Note that for a system with fixed and, the direction of the main lobe depends essentially on λ and the phase shifts. Hence, as in linear networks, the use of delays instead of phase shifts makes the direction of the main lobe independent of frequency [14]. This other degree of freedom will be widely exploited in massive MIMO in 5G. Beamforming, therefore, consists of summing all the signals from the elementary antennas after delaying each signal to compensate for the arrival delay of the incident wave plane on each antenna in the array. The target direction of the main lobe is orthogonal to the plane of the incident wave passing through the target source. In other words, it is a matter of summing in phase the signal of all the elementary antennas in an array to point the main lobe in the desired direction (θ, φ).

This method requires a system of variable delays to be associated with each elementary antenna in the array, the complexity and cost of which are prohibitive. A phase shift is

equivalent to a delay (at a given frequency), and phase shifts generally replace delays. The result is a synthesized beam since there is no real physical lobe. The calculation of the amplitude and phase weights to be assigned to each elementary antenna signal in the array is called pointing weight calculation.

For a digital phase shift, the signal from an elementary antenna k has amplitude:

$$A_k = \sqrt{{R_k}^2 + {I_k}^2} \quad (11)$$

and phase:

$$\psi_k = \tan^{-1}\frac{I_k}{R_k}. \quad (12)$$

If is the weight (amplitude/phase) assigned to the antenna, the amplitude is:

$$B_k = \sqrt{{Wr_k}^2 + {WI_k}^2} \quad (13)$$

and phase:

$$\beta_k = \tan^{-1}\frac{WI_k}{Wr_k} \quad (14)$$

is the signal from the elementary antenna corrected by the pointing coefficients to target the direction(θ,φ).

As mentioned above, in this article, we will discuss the simulation results for 3 scenarios:

- M and N even
- M and N odd
- M even and N odd
- odd M and even N

D1 is directionality based solely on the field above the X-Y plane

D2 is directivity based only on the field below the X-Y plane.

3. Results and Discussion

3.1. Case 1 (M and N even)

We consider M=32 and N=16 for θ=30° and φ=45°

Table 1. Evolution of directivity, progressive phases βx, βy and HPBW for M=32 and N=16 for θ=30° and φ=45°

	N	dx	dy	ßx (°)	ßy (°)	HPBW1 et 2 (°)	D1 (dB)	D2 (dB)
32	16	0.5	0.25	-63.6396	-31.8198	13.3679	15.0059	18.0162
32	16	0.5	0.5	-63.6396	-63.6396	11.8362	17.857	20.8673
32	16	0.5	0.75	-63.6396	-95.4594	10.0807	16.3513	19.3616
32	16	0.5	1	-63.6396	-127.2792	8.5394	17.3457	20.356
32	16	0.25	0.5	-31.8198	-63.6396	17.175	14.9086	17.9189
32	16	0.5	0.5	-63.6396	-63.6396	11.8302	17.857	20.8673
32	16	0.75	0.5	-95.4594	-63.6396	8.5939	16.5755	19.5858
32	16	1	0.5	-127.2792	-63.6396	6.6616	17.3428	20.3531

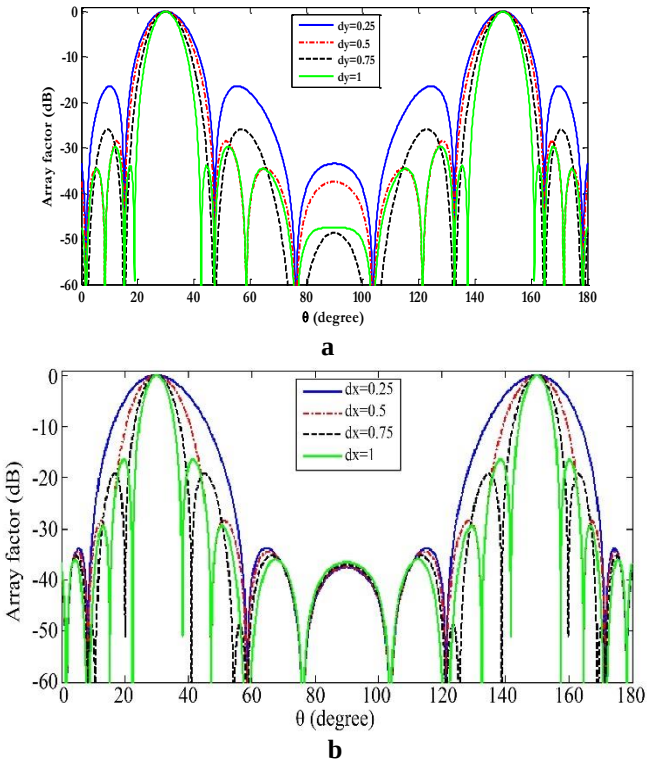

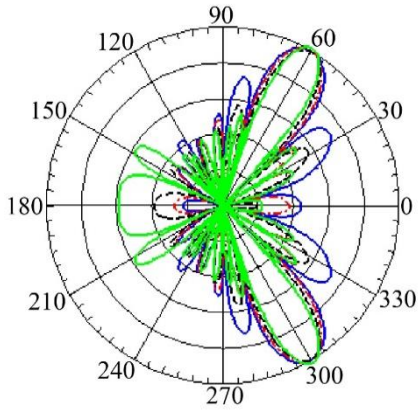

Fig. 4 array factor for (a) Variation of dy, dx set, (b) Variation of dx, dy set and (c) Radiation pattern for M=32 and N=16 for θ=30° and φ=45°.

We can observe that, in addition to the 02 main lobes appearing at -60 and 60, another main lobe covering a user or group of users appears at 180 (typical radiation of an End-Fire network array antenna). This behavior was observed whatever the even values of M and N. We can, therefore, generalize by saying that a planar grating with M and N even elements always admit a 180 main lobe, whatever the desired beam orientation.

3.2. 2nd case (odd M and N)

We consider M=25 and N=9 for θ=30° and φ=45°

Table 2. Evolution of directivity, progressive phases βx, βy and HPBW for M=25 and N=9 for θ=30° and φ=45°

M	N	dx	dy	ßx (°)	ßy (°)	HPBW1 et 2 (°)	D1 (dB)	D2 (dB)
25	9	0.5	0.25	-63.6396	-31.8198	9.5586	17.0434	20.0537
25	9	0.5	0.5	-63.6396	-63.6396	8.8111	19.8456	22.8559
25	9	0.5	0.75	-63.6396	-95.4594	7.848	18.4344	21.4447
25	9	0.5	1	-63.6396	-127.2792	6.8899	19.4074	22.4177
25	9	0.25	0.5	-31.8198	-63.6396	13.8292	16.916	19.9263
25	9	0.5	0.5	-63.6396	-63.6396	8.8111	19.8456	22.8559
25	9	0.75	0.5	-95.4594	-63.6396	8.4235	18.8318	21.8421
25	9	1	0.5	-127.2792	-63.6396	6.5827	19.386	22.3963

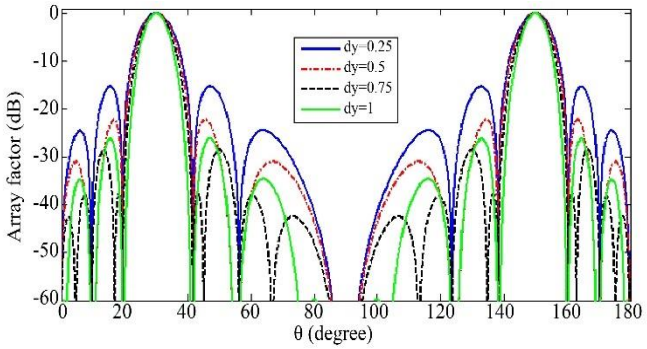

a

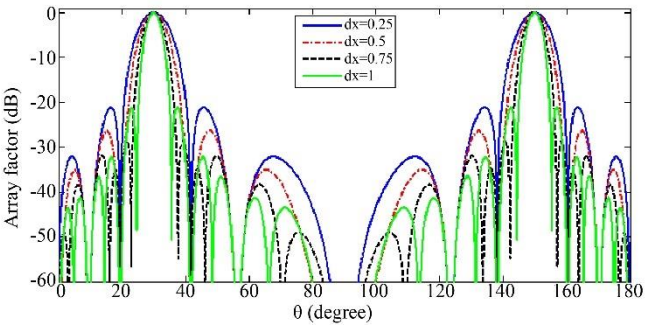

b

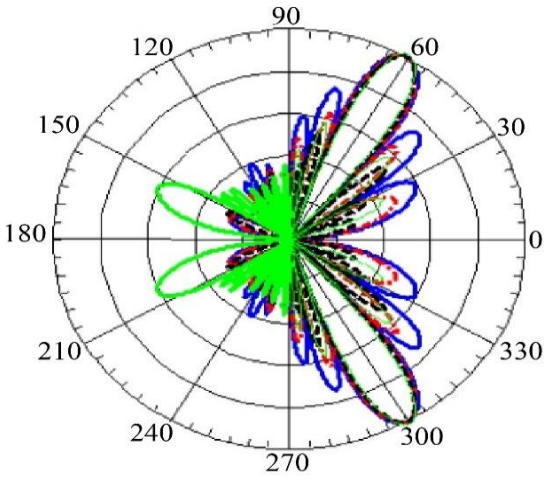

c

Fig.5 array factor for (a) Variation of dy, dx set, (b) Variation of dx, dy set and (c) Radiation pattern for M=25 and N=9 for θ=30° and φ=45°

On the other hand, when M and N become odd, this radiation, like that of a linear End-Fire network, is totally destroyed, whether at 0 or 180 degrees. This observation was made regardless of the odd values of M and N.

3.3. 3rd case (even M and odd N)

We consider M=32 and N=9 for θ=30° and φ=45°

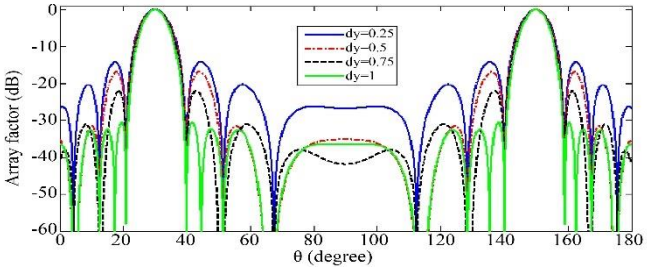

a

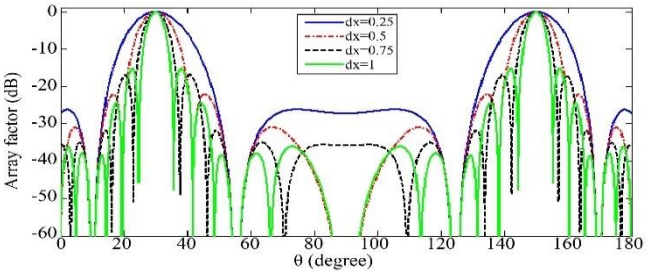

b

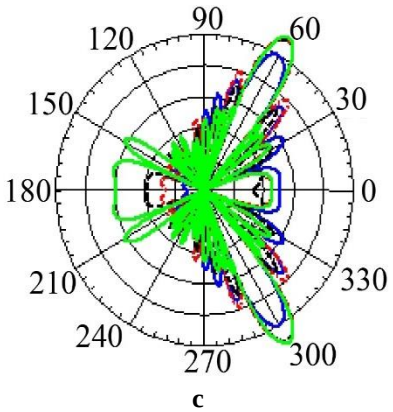

c

Fig. 6 array factor for (a) Variation of dy, dx set, (b) Variation of dx, dy set and (c) Radiation pattern for M=32 and N=9 for θ=30° and φ=45°

The situation becomes totally different when, for even-numbered M and odd-numbered N, the radiation outside the desired pointing directions is like that of an end-fire linear array, i.e. the principal lobes emerge at 0 and 180 respectively, whatever the even-numbered M or odd-numbered N value.

Table 3. Evolution of directivity, progressive phases βx, βy and HPBW for M=32 and N=9 for θ=30° and φ=45°

M	N	dx	dy	ßx (°)	ßy (°)	HPBW1 et 2 (°)	D1 (dB)	D2 (dB)
32	9	0.5	0.25	-63.6396	-31.8198	8.2516	16.6969	19.7072
32	9	0.5	0.5	-63.6396	-63.6396	7.9491	19.469	22.4793
32	9	0.5	0.75	-63.6396	-95.4594	7.5014	17.9177	20.928
32	9	0.5	1	-63.6396	-127.2792	6.9731	19.0533	22.0636
32	9	0.25	0.5	-31.8198	-63.6396	13.9975	16.5442	19.5545
32	9	0.5	0.5	-63.6396	-63.6396	7.9491	19.469	22.4793
32	9	0.75	0.5	-95.4594	-63.6396	5.4422	18.3435	21.3538
32	9	1	0.5	-127.2792	-63.6396	4.121	18.9878	21.9981

3.4. 4th case (odd M and even N)

We consider M=9 and N=20 for θ=30° and φ=45°

Table 4. Evolution of directivity, progressive phases βx, βy and HPBW for M=9 and N=20 for θ=30° and φ=45°

M	N	dx	dy	ßx (°)	ßy (°)	HPBW1 et 2 (°)	D1 (dB)	D2 (dB)
9	20	0.5	0.25	-63.6396	-31.8198	12.7061	17.6393	20.1315
9	20	0.5	0.5	-63.6396	-63.6396	7.7023	20.5842	23.5945
9	20	0.5	0.75	-63.6396	-95.4594	5.3625	19.7269	22.7372
9	20	0.5	1	-63.6396	-127.2792	4.0864	20.0628	23.0731
9	20	0.25	0.5	-31.8198	-63.6396	8.1821	17.7774	20.7877
9	20	0.5	0.5	-63.6396	-63.6396	7.7023	20.5842	23.5945
9	20	0.75	0.5	-95.4594	-63.6396	7.0428	19.1473	22.1576
9	20	1	0.5	-127.2792	-63.6396	6.334	20.1315	23.1418

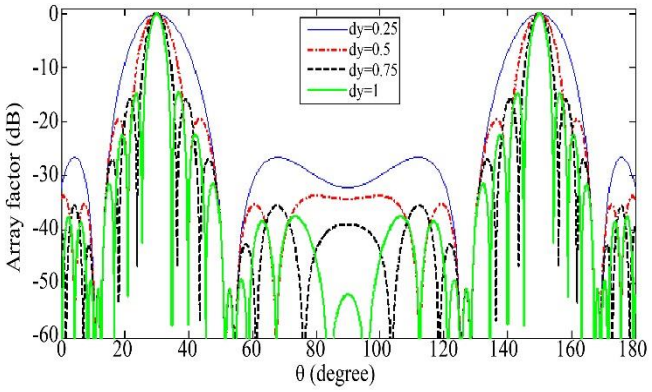

a

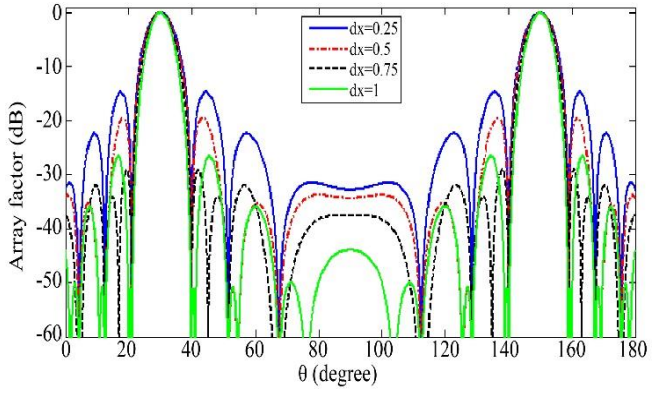

b

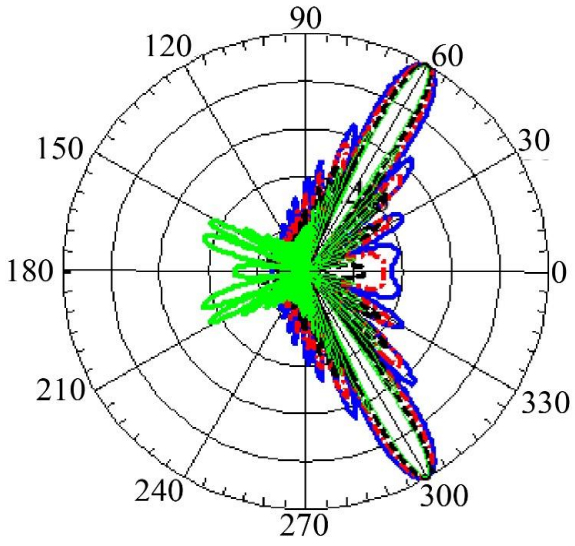

c

Fig. 7 array factor for (a) Variation of dy, dx set, (b) Variation of dx, dy set and (c) Radiation pattern for M=9 and N=20 for θ=30° and φ=45°

On the other hand, when the order of M and N is reversed, i.e. M becomes odd and N even, outside the desired direction of coverage, the only remaining primary lobe of the End-Fire network is now at 0 only. The 180-degree lobe has left its place to the secondary lobes, whatever the odd values of M and even values of N.

3.5. 5th case (M and N equal and even)

We consider M=9 and N=20 for θ=30° and φ=45°

Table 5. Evolution of directivity, progressive phases βx, βy and HPBW for M=32 and N=32 for θ=30° and φ=45°

M	N	dx	dy	ßx (°)	ßy (°)	HPBW1 et 2 (°)	D1 (dB)	D2 (dB)
32	32	0.5	0.25	-63.6396	-31.8198	7.5596	21.1784	24.1887
32	32	0.5	0.5	-63.6396	-63.6396	6.0139	24.1259	27.1362
32	32	0.5	0.75	-63.6396	-95.4594	4.7031	23.9085	26.9188
32	32	0.5	1	-63.6396	-127.2792	3.7762	23.5787	26.589
32	32	0.25	0.5	-31.8198	-63.6396	7.5596	21.2131	24.2234
32	32	0.5	0.5	-63.6396	-63.6396	6.0139	24.1259	27.1362
32	32	0.75	0.5	-95.4594	-63.6396	4.7031	23.848	26.8583
32	32	1	0.5	-127.2792	-95.4594	3.3954	23.6437	26.654

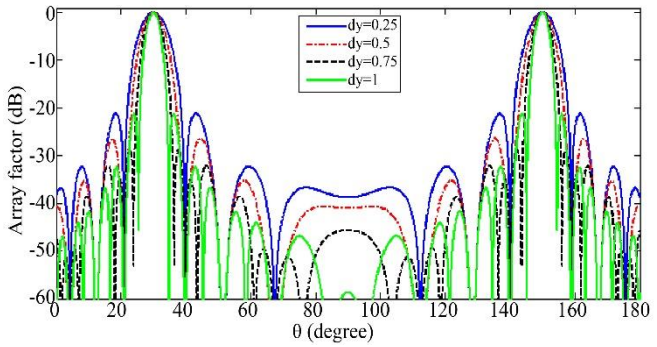

a

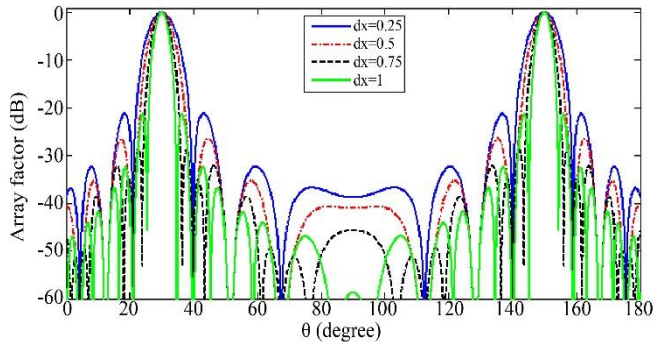

b

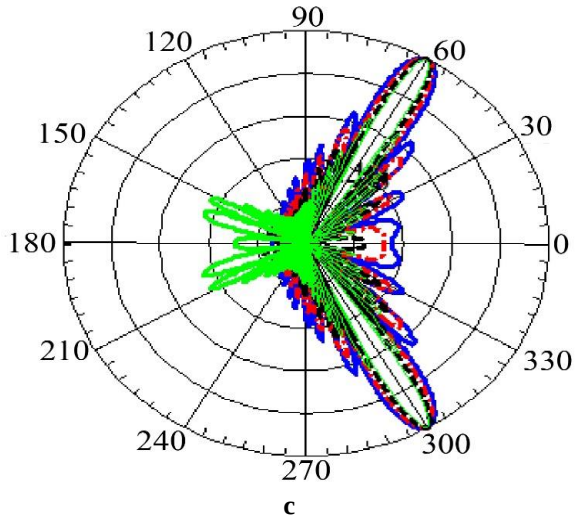

c

Fig. 8 array factor for (a) Variation of dy, dx set, (b) Variation of dx, dy set and (c) Radiation pattern for M=32 and N=32 for θ=30° and φ=45°.

This last case is the most interesting of all and has received the most attention not only in the literature but also from most manufacturers, such as Huawei and NOKIA, for practical implementation in Massive MIMO stations. In fact, the perfect symmetry of this configuration in terms of network factor makes it the perfect candidate. So we will have configurations like 32TX/32TR or 64TX/64TR. Overall, it can be seen from the above that whatever the scenario chosen, the radiation pattern of a planar array is identical to the radiation pattern of a Broadside array, except for one orientation. Indeed, a linear Broadside array always has 2 main lobes oriented at -90° and 90° respectively. By analogy of observation of the fields above and below the X-Y plane, we can see the same symmetry of main lobes on the planar array (at θ=60° in our case). This validates our initial hypothesis that the direct analytical method uses the classical beamforming mechanisms known from the Broadside base linear grating. What is more, non-negligible main lobes appear at the End-Fire (at 0° and/or 180°), depending on whether M is even or N is odd, and vice-versa. It is this degree of freedom that is exploited in 5G Massive MIMO for cooperative base stations, for example. In fact, the principle consists of using the same base station to simultaneously serve 2 users located in 2 different cells, sometimes with different traffic and service quality requirements. Similarly, HPBW and the progressive phase tend to decrease as they increase. βi tends to remain unchanged when it is fixed. Meanwhile, D2 directivity based solely on the field below the X-Y plane becomes more directional as the number of grating elements increases. This advantage is widely exploited in 5G Massive MIMO applications for IoT and radar to track moving targets. However, particular attention needs to be paid when designing these networks for certain applications, especially when the network pitch approaches or reaches a value equal to a wavelength. In the latter case, a considerable number of sidelobes may appear on the grating factor or radiation pattern. In most cases, these secondary lobes represent energy lost through radiation, and their number is proportional to the energy lost.

4. Conclusion

Unlike linear arrays, which have their greatest impact when the array pitch or the distance between sources in the

design is of the order of 0.5λ, planar arrays offer a much wider range of applications because of the array factor, radiation pattern and directivity results obtained whatever the array pitch considered. The design of these gratings is much more interesting when M and N are equal and even. This is the configuration used by most designers of massive MIMO antennas, such as Huawei and NOKIA, to name but a few. In all fairness, these results can be widely exploited in design, whether the network pitch is between 0.25λ and λ or whether the number of radiating elements is increasing. This impressive number of degrees of freedom makes the planar source network the ideal candidate for equipping massive MIMO stations in 5G and beyond. In addition to these advantages, the fact that the results are exploitable, whatever the network step, opens up a new avenue of research for the application of this technology to frequency bands not yet popularized, such as E-Band and D-Band. This other approach could be the subject of further research in the future.

Funding Statement

The University of Douala financially supported the research and publication from the budget line of the Laboratory of Technology and Applied Sciences (LTSA).

References

[1] Thomas L. Marzetta et al., *Fundamentals of Massive MIMO*, Cambridge University Press, 2016. [Google Scholar] [Publisher Link]

[2] Barry D. Van Veen, and Kevin M. Buckley, "Beamforming: a Versatile Approach to Spatial Filtering," *IEEE ASSP Magazine*, vol. 5, no. 2, pp. 4-24, 1988. [CrossRef] [Google Scholar] [Publisher Link]

[3] Wonil Roh et al., "Millimeter-Wave Beamforming as an Enabling Technology for 5G Cellular Communications: Theoretical Feasibility and Prototype Results," *IEEE Communications Magazine*, vol. 52, no. 2, pp. 106-113, 2014. [CrossRef] [Google Scholar] [Publisher Link]

[4] Robert W. Heath Jr, Comparing Massive MIMO and mmWave MIMO, The University of Texas at Austin, 2014. [Online]. Available: https://ctw2014.ieee-ctw.org/slides/session3/Heath-CTW_v6.pdf

[5] George R. MacCartney Jr. et al., "Millimeter Wave Wireless Communications: New Results for Rural Connectivity," *ATC '16: Proceedings of the 5th Workshop on All Things Cellular: Operations, Applications and Challenges*, USA, pp. 31-36, 2016. [CrossRef] [Google Scholar] [Publisher Link]

[6] Jeffrey G. Andrews et al., "Modeling and Analyzing Millimeter Wave Cellular Systems," *IEEE Transactions on Communications*, vol. 65, no. 1, pp. 403-430, 2017. [CrossRef] [Google Scholar] [Publisher Link]

[7] Sylvain Collonge, Gheorghe Zaharia, and Ghais El Zein, "Influence of the Human Activity on Wide-Band Characteristics of the 60 GHz Indoor Radio Channel," *IEEE Transactions on Wireless Communications*, vol. 3, no. 6, pp. 2396-2406, 2004. [CrossRef] [Google Scholar] [Publisher Link]

[8] Fred W. Smith, "Design of Quasi-Optimal Minimum-Time Controllers," *IEEE Transactions on Automatic Control*, vol. 11, no. 1, pp. 71-77, 1996. [CrossRef] [Google Scholar] [Publisher Link]

[9] Bernard Widrow et al., "Adaptive Antenna Systems," *Proceedings of the IEEE*, vol. 55, no. 12, pp. 2143-2159, 1967. [CrossRef] [Google Scholar] [Publisher Link]

[10] Frank Gross, *Smart Antenna for Wireless Communication*, McGraw-Hill Education, pp. 1-288, 2005. [Google Scholar] [Publisher Link]

[11] Tapan K. Sarkar et al., *Smart Antennas*, Wiley-IEEE Press, pp. 1-472, 2005. [Google Scholar] [Publisher Link]

[12] Matthew N.O. Sadiku, *Numerical Techniques in Electromagnetics*, CRC Press, pp. 1-743, 2001. [Google Scholar] [Publisher Link]

[13] J. Koford, and Gabriel F. Groner, "The Use of an Adaptive Threshold Element to Design a Linear Optimal Pattern Classifier," *IEEE Transactions on Information Theory*, vol. 12, no. 1, pp. 42-50, 1966. [CrossRef] [Google Scholar] [Publisher Link]

[14] John Litva, and Titus Lo, *Digital Beamforming in Wireless Communications*, Artech House, pp. 1-301, 1996. [Google Scholar] [Publisher Link]